Preprints of the 19th World Congress
The International Federation of Automatic Control
Cape Town, South Africa. August 24-29, 2014

Modeling of the Master Laser Oscillator Phase Noise for the European XFEL using Fractional Order Systems

Michael Heuer * **Gerwald Lichtenberg** ** **Sven Pfeiffer** *
Holger Schlarb * **Christian Schmidt** * **Herbert Werner** ***

* *Deutsches Elektronen Synchrotron Hamburg, Notkestraße 85, 22607 Hamburg, Germany (e-mail: {michael.heuer, sven.pfeiffer, holger.schlarb, christian.schmidt}@desy.de).*
** *Hamburg University of Applied Sciences, Ulmenliet 20, 21033 Hamburg, Germany (e-mail: gerwald.lichtenberg@haw-hamburg.de)*
*** *Hamburg University of Technology, Schwarzenbergstraße 95, 21073 Hamburg, Germany (e-mail: h.werner@tu-harburg.de)*

Abstract: The European X-ray Free-Electron Laser will generate high energy light pulses in the femto-second range. A clock signal, which synchronizes all components, is distributed via laser pulses. The accuracy of these laser pulses is crucial to achieve precise measurements which are needed to control the Free-Electron Laser. In order to reach the maximum performance, advanced model-based control approaches are used to compensate external influences. This paper shows the modeling of the Master Laser Oscillator by fractional order systems, which improve known approaches to system modeling by providing a higher accuracy.

Keywords: Modelling, Fractional Order Systems, Free-Electron Laser

1. INTRODUCTION

At the Deutsches Elektronen Synchrotron (DESY) in Hamburg, Germany, the European X-ray Free-Electron Laser (XFEL) is under construction. This linear accelerator with a length of 3.5 km will generate extremely intense and short X-ray laser light pulses with a duration in the femto-second range and wavelength down to 0.05 nm. To generate these light pulses, electron bunches are accelerated up to an energy of 17.5 GeV and lead through an undulator which forces the electrons to emit X-ray laser pulses. Further technical specifications of the facility can be found in Brinkmann et al. (2007). These intense and ultra-short X-ray laser pulses provide physicist from all over the world a light source to take a closer look into tiny structures on atomic scale. It will be possible to reveal how complex biomolecules are assembled or, due to the high repetition rate of maximum 4.5 MHz, even to film the folding and formation of such molecules, Günther et al. (2011). Such measurements require a timing signal with an error in femto-second range for all components within the free-electron laser. One of the main challenges is to fulfill this requirement.

Usually, a synchronization signal is distributed via an electric signal by coaxial cables. For long distances in kilometer-range, this signal needs to be frequently amplified due to damping of the cable itself, an additional noise source would be included and hereby this is not suitable for high precision synchronization system. A laser based synchronization system for large-scale timing distribution was proposed in Kim et al. (2004), is used for the Free electron LASer in Hamburg (FLASH), and will be used for XFEL, Schulz et al. (2013).

In such a synchronization system a Master Laser Oscillator (MLO) generates a laser pulse train, which is used as the timing signal. To control this laser a so-called Phase Locked Loop (PLL) is used. The linear time invariant model of a PLL is analyzed in Rubiola (2009) and from the control theory point of view in Abramovitch (2003). In Gardner (2005) it is shown that the noise shape, whose integral is one performance criterion, does not fit the $n \cdot 20\,\mathrm{dB}$ rule known for LTI systems. Moreover, fractional order controller, also known as CRONE controller, see Oustaloup (1991), have a superior behavior, compared to their LTI counterparts, e.g. shown in El-Khazali et al. (2007) an Xue et al. (2006). This motivates the usage of a fractional order model to describe this plant with its main noise influences. An overview of fractional order systems is given in Monje et al. (2010), Das (2008) and Chen et al. (2009). The paper shows how to build such a model, which can then be used in a model based controller synthesis.

This paper is organized as follows: Section 2 gives an overview of the planed laser synchronization system. The modeling of the MLO is shown in Section 3, where the system is derived and extended to include the occurring oscillator phase noise using fractional order models as noise shape filters. Section 4 shows the identification of the model parameters for the currently used system at FLASH, followed by the simulation results in Section 5 and a conclusion and outlook completes the paper.

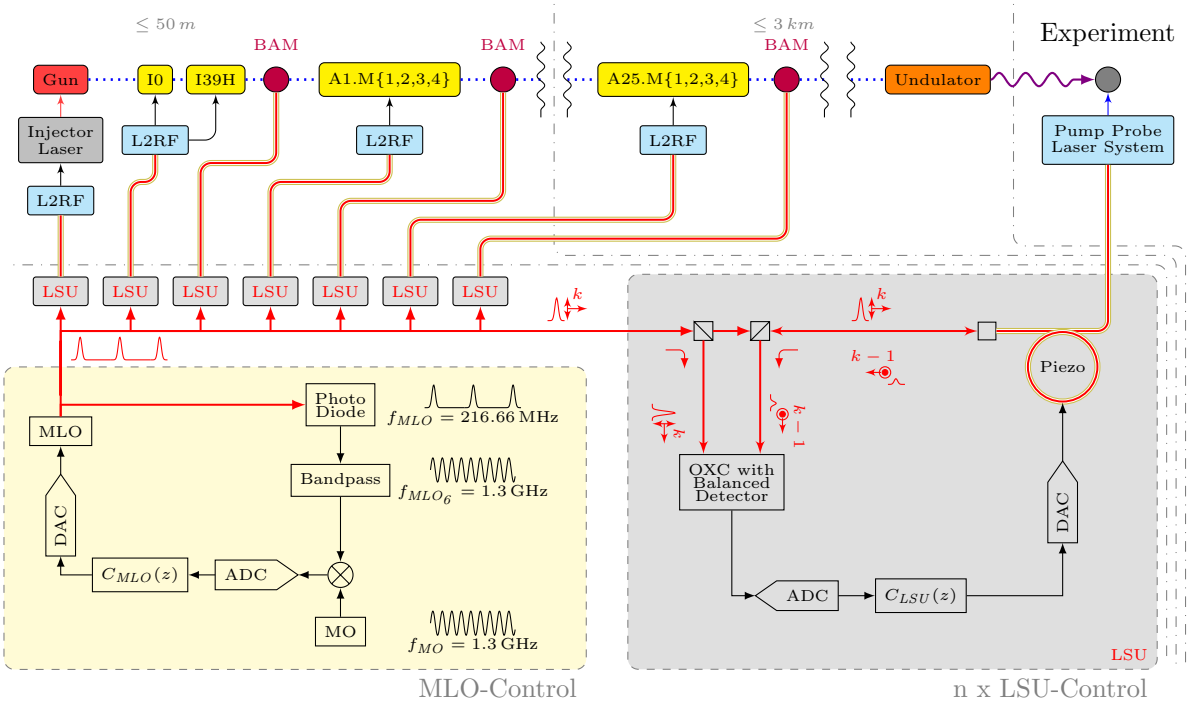

Fig. 1. Overview of the European XFEL and the connected laser based synchronization system, including the Master Laser Oscillator (MLO) and the Link Stabilizing Units (LSU).

2. LASER BASED SYNCHRONIZATION SYSTEM OVERVIEW

A simplified diagram of the laser based synchronization system with the main part of the accelerator, the beamline, is given in Fig. 1. The injector laser triggers a detachment of electrons at the cathode of the gun. This electron bunch with a charge up to 1 nC is accelerated by 101 superconducting cryomodules (I0 and I39H, A1.M1-4, . . . , A25.M1-4) up to its final energy. A more detailed explanation of this modules is given in Pfeiffer et al. (2011). At the end of the beamline the bunch is lead through the undulator, a periodic arrangement of magnets, which forces the electron bunches on a sinusoidal trajectory in its transverse direction. This causes the so-called Self-Amplified Spontaneous Emission (SASE) process, which generates the high energy X-ray pulse. Other important devices are, for example, the Laser to Radio Frequency converter (L2RF), which is used to connect the electrical systems to the optical synchronization system. The Bunch Arrival time Monitor (BAM) is used to measure the relative time of electron bunches crossing a certain position in the beamline w.r.t. the synchronization system within a femto-second precision, see Bock (2012).

To provide a clock signal to these devices the laser based synchronization system is used. It consists of two parts, the Master Laser Oscillator (MLO), which generates the laser pulse train, i.e. the timing signal of the system, and the Link Stabilizing Units (LSU), which are responsible to stabilize the up to 3.5 km long fiber link through which the pulse train is feed from the synchronization hutch at the beginning of the accelerator to the different devices.

The lower right part of Fig. 1 shows the control scheme of a LSU. If a pulse enters the LSU, a small fraction of the laser pulse is branched off and the main part goes through a piezo stretcher into the fiber to the device in the accelerator. A piezo stretcher allows to slightly change the length of the fiber, hence it is used as an actuator in this scheme. At the device the pulse is partly reflected and travels back the way to the LSU. This returning pulse and the fraction of the subsequent pulse are correlated twice in an Optical Cross Correlator (OXC). Inside the OXC both polarizations have different velocity and therefore the correlations are different. A balanced detector can measure the timing difference between these two pulses by measuring the difference between both correlations. If the pulses within the pulse train are equidistant and the signal of the balanced detector is zero, the length of the attached fiber is a multiple of the MLO repetition rate added with a constant bias. With this scheme it is possible to suppress the error of the timing signal induced by length changes of the fiber caused by stress, temperature and/or humidity changes acting on the fiber. The performance of this control unit dependents first of all on a very precise frequency of the laser pulse train, generated by the MLO.

The MLO control scheme is shown in the lower left part of Fig. 1. This is the main component of the laser synchronization system and provides the stable laser pulse train at a repetition rate of 216.66 MHz [1], which is used as the clock signal for synchronization. A variation in this frequency has a direct influence on the sampling quality of all attached devices and on the control performance of the LSUs. Therefore it is necessary to stabilize the frequency of the MLO and suppress all possible noise sources. This noise suppression is done via a locking against the RF-Master Oscillator (MO) of the facility.

[1] The sixth harmonic of the main Master Oscillator (MO) at 1.3 GHz

3. MODELING OF THE MLO

In this section a model for the MLO control scheme shown in Fig. 1 is derived. The signals denoted with a tilde are high frequency sinusoidal clock signals, whereas the ones without are the down-sampled signals only describing a phase relation.

As light source for the MLO a laser with a center wavelength of 1550 nm with a pulse repetition rate of 216.66 MHz is chosen. Special properties of this laser are a pulse duration of less than 100 fs, an average power up to 120 mW and an amplitude noise of less than 0.2% (rms). A wavelength of 1550 nm is often used in telecommunication industries, therefore a wide spectrum of components is available.

To tune the repetition rate of the laser, one can either use a piezo crystal or the temperature expansion of a beam. It is known, that a piezo crystal has a higher bandwidth and it is obvious to expect much better results with this actuator for the frequency tuning. Therefore this input is chosen as the control input $u(t)$ for the laser. The band pass filtered output of the laser is given as sinusoidal signal $\tilde{y}(t)$, where the frequency of this signal is adjustable by the laser input.

The scheme of the control loop used to stabilize the repetition rate of this laser is called Phase Locked Loop and will be described in the following subsection.

3.1 Phase Locked Loops

Phase Locked Loops have a wide field of application and one can find them in almost every modern electronic device such as mobile phones, laptops or other components with micro controllers.

In general, those are used to synchronize one frequency with respect to an other. Fig. 2 shows the structure of a general PLL as described in Gardner (2005).

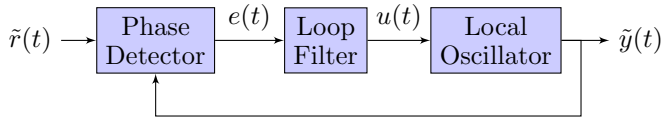

Fig. 2. Block diagram of a Phase Locked Loop

The Local Oscillator generates a sinusoidal signal $\tilde{y}(t)$ which has to be synchronous to the sinusoidal reference signal $\tilde{r}(t)$. If the phase error $e(t)$, generated by the phase detector, is zero over time, the two signals are equal in frequency and phase. This error signal is used by the controller, here called Loop Filter, to generate a control value adjusting the Local Oscillator frequency in a way, that the phase error goes to zero.

The setup is shown in the lower left part of Fig. 1. To get an electrical signal of the 216.66 MHz light pulses, a photo diode and bandpass filter are used to measure the sixth harmonic (1.3 GHz) of the pulse train. The resulting signal is mixed with the MO signal.

The nonlinear equations describing the system, similar to the ones in Abramovitch (2003), are

$$\tilde{r}(t) = \sin(\omega_{MO} t)\,, \tag{1}$$
$$\tilde{y}(t) = a\cos(\omega_{LO}(t)t + \phi(t) + \phi_n(t))\,, \tag{2}$$
$$\tilde{e}(t) = \tilde{r}(t)\tilde{y}(t), \tag{3}$$
$$= \frac{a}{2}\underbrace{\sin((\omega_{MO}+\omega_{LO}(t))t + \phi(t) + \phi_n(t))}_{\gamma_{high}} + \frac{a}{2}\underbrace{\sin((\omega_{MO}-\omega_{LO}(t))t - \phi(t) - \phi_n(t))}_{\gamma_{low}}\,, \tag{4}$$
$$\dot{\phi}(t) = \omega_{MO} - \omega_{LO}(t)\,, \tag{5}$$
$$\phi(0) = \phi_0\,, \tag{6}$$

where $\tilde{r}(t)$ is the signal from the MO with the angular frequency $\omega_{MO} = 2\pi \cdot 1.3\,\text{GHz}$. The signal $\tilde{y}(t)$ generated by the laser pulse train with an angular frequency $\omega_{LO}(t)$, phase shift $\phi(t)$ and noise $\phi_n(t)$ acting on the phase shift.

In order to linearize the system, the following commonly used assumptions, as in Abramovitch (2003), are used:

1. The system is close to the operating point $|\omega_{MO} - \omega_{LO}(t)| \to 0$
2. There are just small phase changes $\sin(\phi(t)) \approx \phi(t)$
3. High order harmonics are low pass filtered and therefore vanished, $\gamma_{high} \to 0$
4. An input to the local oscillator leads to a linear change around the operating point $\omega_{LO}(t) = ku(t) + \omega_{MO}$

The first assumption allows us to just take a look at the frequency differences, i.e. $r(t)$ as the reference phase and $y(t)$ as the output phase, both with respect to the sinusoidal signal $\tilde{r}(t)$. Assumption 1. and 2. are used to linearize γ_{low} and together with 3. to linearize (4). The last assumption sets the piezo transfer function to a constant gain, which is valid if the piezo is much faster than the frequency changes.

With this simplifications the linearized system dynamics can be described by an integrator, i.e. in time domain as

$$\dot{\phi}(t) = -ku(t)\,, \tag{7}$$
$$e(t) = -\frac{a}{2}(\phi(t) + \phi_n(t))\,, \tag{8}$$

and in frequency domain as

$$G(s) = \frac{E(s)}{U(s)} = \frac{ak}{2s}\,. \tag{9}$$

This shows, as expected, that the phase shift $\phi(t)$ between both frequencies and therefore the error $e(t)$ will diverge if both frequencies are not equal.

3.2 Phase Noise and Timing Jitter

An ideal oscillator has a Dirac impulse as its frequency spectrum. This is not true in real world measurements. Fig. 3 shows an ideal and a real oscillator. The real oscillator spectrum has components near the center frequency f_c, due to a noise term $\phi_n(t)$ on the phase. This noise term at the MLO output directly influences the zero crossing of timing pulse and acts as a disturbance to the LSU OXC measurement. Therefore it is crucial for the precise sampling of the connected devices in the accelerator.

To measure the term $\phi(t) + \phi_n(t)$ one can mix the noisy oscillator signal $\tilde{y}(t)$ with an ideal one $\tilde{r}(t)$ as shown in

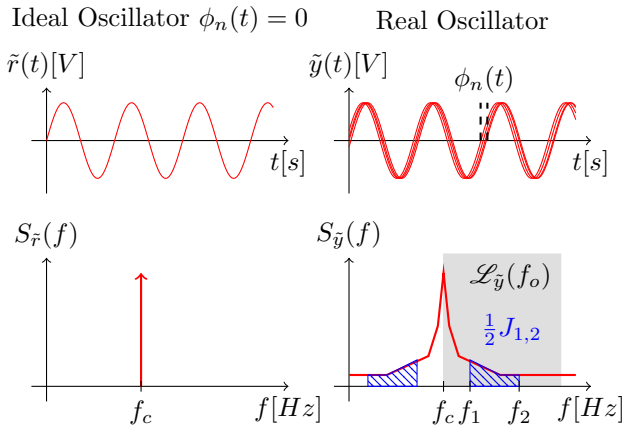

Fig. 3. Time (upper subplot) and frequency (lower subplot) domain behavior of an ideal and a real oscillator

Fig. 4. In this case this is what the phase detector of the MLO, described in the last section, does and with the linearizations the noise term is equal to the measured phase error signal $e(t)$.

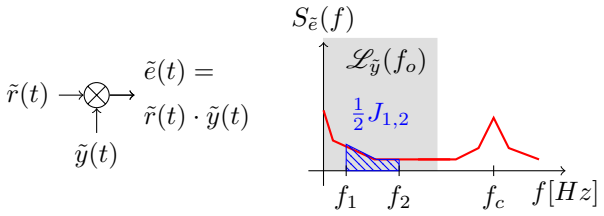

Fig. 4. Frequency domain behavior of an ideal oscillator mixed with a real oscillator

The root mean square value of this error signal is called timing jitter J. It can be calculated in the time or in the frequency domain by using the theorem of Parseval as

$$J_{rad}^2 = \|\phi_n(t)\|_{rms}^2 = \int_{-\infty}^{\infty} |\phi_n(t)|^2 \,\mathrm{d}t$$
$$= \int_{-\infty}^{\infty} |\hat{S}_{\phi_n}(f)|^2 \,\mathrm{d}f = \int_{-\infty}^{\infty} S_{\phi_n}(f) \,\mathrm{d}f\,, \qquad (10)$$

where $S_{\phi_n}(f)$ is the power density spectrum of $\phi_n(t)$.

The jitter in the unit seconds, with the carry frequency f_c, is

$$J_s = \frac{J_{rad}}{2\pi f_c}\,. \qquad (11)$$

Under the assumption that there is only phase and no amplitude noise, the spectrum $S_{\tilde{y}}(f)$ of the signal $\tilde{y}(t)$ is symmetric around the center frequency f_c. Therefore, as described in Gardner (2005), only one side of the spectrum near the center frequency is considered for the characterization, the so-called single-sided phase noise spectrum

$$\mathscr{L}_{\tilde{y}}(f_o) = \frac{S_{\tilde{y}}(f_o + f_c)}{2}, \quad \forall f_o > 0\,, \qquad (12)$$

which is a function of the offset frequency f_o.

Due to the mixing and low pass filtering, the power density spectrum of $e(t)$ is equal to the phase noise spectrum:

$$\mathscr{L}_{\tilde{y}}(f_o) = S_e(f)\,. \qquad (13)$$

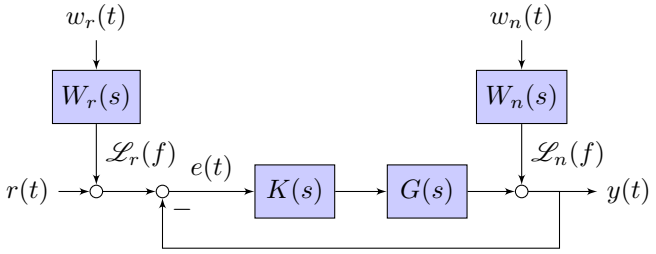

Fig. 5. Block diagram of the linearized system including the noise shaping filters $W_r(s)$ for the MO and $W_n(s)$ for the MLO

The output jitter in a certain frequency range

$$J_{rad,f_1,f_2} = \sqrt{2\int_{f_1}^{f_2} \mathscr{L}(f)\,\mathrm{d}f}, \quad 0 < f_1 < f_2 \qquad (14)$$

is commonly used to compare performances of oscillators and depends on the integration bounds. It is not possible to take ranges from 0 to ∞, because this jitter would always go to infinity, caused by a constant bias of the spectrum called noise floor which is unavoidable due to thermal noise effects [2], hence a principle performance bound.

To model the noise $\mathscr{L}_r(f)$ and $\mathscr{L}_n(f)$ of the plant, the assumption that the reference oscillator is ideal is dropped, because it is also influenced by phase noise. Fig. 5 shows the resulting structure with the noise shape filters $W_r(s)$ for the MO and $W_n(s)$ for the MLO, respectively, both fed with white gaussian noise $\omega_r(t)$ and $\omega_n(t)$. The arising question is:

- How to choose the filter functions $W_r(s)$ and $W_n(s)$, that the noise $\mathscr{L}_r(f)$ and $\mathscr{L}_n(f)$ fits with the measured power density spectrum.

The propagation of an input power density spectrum $S_u(\omega)$ trough a linear time invariant system $H(j\omega)$ results in an output power density spectrum

$$S_y(\omega) = |H(j\omega)|^2 S_u(\omega)\,. \qquad (15)$$

From (10) and (15) follows, that if a zero mean unit variance white noise signal $u(t)$ with $S_u(f) = 1$, propagates through an LTI system, the rms value of the output signal $y(t)$ is given by

$$\|y(t)\|_{rms}^2 = \frac{1}{2\pi}\int_{-\infty}^{\infty} S_y(\omega)\mathrm{d}\omega$$
$$= \frac{1}{2\pi}\int_{-\infty}^{\infty} |H(j\omega)|^2 \mathrm{d}\omega = \|H(s)\|_2^2\,, \qquad (16)$$

which is the $\mathcal{H}_2$ norm of the system $H(s)$.

Choosing the noise filters as

$$|W_r(s)|^2 = \mathscr{L}_r(f) \quad \text{and} \quad |W_n(s)|^2 = \mathscr{L}_n(f)\,, \qquad (17)$$

the $\mathcal{H}_2$ norm of the system from $w_r(t)$ to $y(t)$ represents the jitter $J_{s,r}$ induced through the MO and the $\mathcal{H}_2$ norm of the system from $w_n(t)$ to $y(t)$ represents jitter $J_{s,n}$ induced through the MLO with [3]

$$J_{s,r} = \frac{\|W_r(s)\|_2}{2\pi f_c} \quad \text{and} \quad J_{s,n} = \frac{\|W_n(s)\|_2}{2\pi f_c}\,. \qquad (18)$$

[2] The thermal noise power is given by $P = k_B T \Delta f$. The noise floor at room temperature is $-174\,\mathrm{dBm/Hz}$.
[3] Remember, that $\omega = 2\pi f$, $\mathrm{d}f = \mathrm{d}\omega(2\pi)^{-1}$

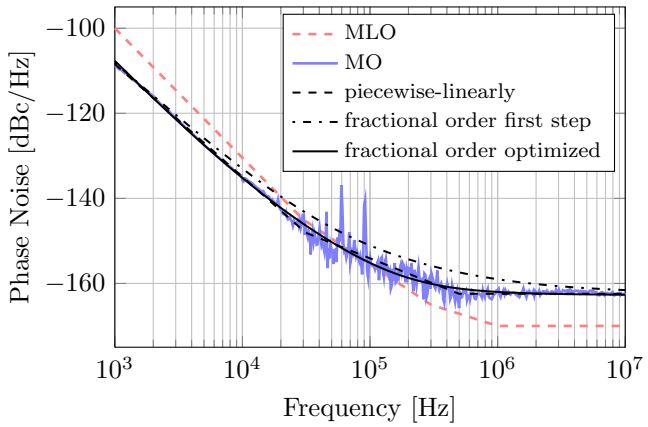

Fig. 6. Measured Phase Noise of the MO (blue, solid) installed at FLASH, expected one of a MLO (red, dashed) and different approximations in black

3.3 Shape of the Phase Noise

To determine the noise filters $W_r(s)$ and $W_n(s)$, the open loop phase noise of the MO was measured. The result (blue, solid) and the theoretical shape of the MLO (red, dashed) are shown in Fig. 6. In the low frequency range the noise power of the MO is much lower than the one of the MLO, which changes for higher frequencies at an intersection point. A controller which minimizes the output jitter would have a good reference tracking up to the frequency of the intersection point even if the bandwidth could be higher.

Another very important aspect is the slope of the graphs. This correspond to different physical effects listed in Rubiola (2009) and for completeness introduced:

Δ dB	$S(f)$	Physical meaning
−30 dB	f^{-3}	Flickering noise on the frequency
−20 dB	f^{-2}	White noise on the frequency
−10 dB	f^{-1}	Flickering noise on the phase
0 dB	1	White noise on the phase

The shape can be piecewise-linearly approximated with stable transfer functions of the type

$$S_l(f) = \frac{k}{f^\alpha + 1} \tag{19}$$

where α correspond to the slope of the element and k gives the crossing with $f = 1$. One point is to keep in mind, that these values are power signals therefore the following rule holds:

$$\Delta P[\text{dB}] = 10 \log_{10} \left(\frac{P_2\,[\text{W}]}{P_1\,[\text{W}]} \right) \tag{20}$$

For that reason a slope of −20 dB leads to a spectral behavior of f^{-2} and due to (15) to a linear system behavior of f^{-1} as commonly known.

Fig. 6 shows, that this system contains parts which does not fit to the $n \cdot 20\,\text{dB}$ rule with $n \in \mathbb{Z}$ for LTI systems. To model this behavior, it is possible to fit the shape with a high order LTI system or use a fractional order system description.

3.4 Fractional Order Systems

The required filter $W_r(s)$, has to hold

$$|W_r(s)|^2 = \frac{k}{s} \Leftarrow W_r(s) = \frac{k^{\frac{1}{2}}}{s^{\frac{1}{2}}}\,, \tag{21}$$

in the frequency domain and has to be stable.

Such systems, where the exponent of the complex variable s is a real value are called fractional order systems, explained in Monje et al. (2010). One example of fractional order control is the $\text{PI}^\lambda\text{D}^\mu$ controller, which extends the PID controller with two new tuning knobs and new possible properties, for example iso-damping where the overshoot is independent of the system gain, shown in Luo and Chen (2012).

Here a first impression is given how the generalization of integration and differentiation looks like. The new fractional operator for n-th integration $\mathscr{D}^{-n}$ looks like Rieman-Lioville's definition:

$$\mathscr{D}^{-n}\{f(t)\} = \frac{1}{\Gamma(n)} \int_0^t f(y)(t-y)^{n-1}\,dy, \quad n \in \mathbb{R}^+\,, \tag{22}$$

with $\Gamma(n)$ as Eulers Gamma function, an extension of the factorial function to real numbers.

The n-th differentiation follows the Grünwald-Letnikov's definition with:

$$\mathscr{D}^{n}\{f(t)\} = \lim_{h\to 0} \frac{1}{h^n} \sum_{k=0}^{n} (-1)^n \binom{n}{k} f(t-kh), \quad n \in \mathbb{R}^+\,. \tag{23}$$

With this definitions the commonly known rules for the Laplace transform $\mathcal{L}\{\cdot\}$ can be extended to cover fractional orders, by

$$\mathscr{D}^{n}\{f(t)\} = s^n \mathcal{L}\{f(t)\}, \quad n \in \mathbb{R}\,. \tag{24}$$

Example: The Laplace transform of a fractional order integrator is given by

$$\mathcal{L}^{-1}\left\{\frac{1}{s^n}\right\} = \frac{t^{n-1}}{\Gamma(n)}, \quad n \in \mathbb{R}\,. \tag{25}$$

One can see that fraction changes to the Gamma function which is reasonable, because this is the generalization of the fraction.

There are a couple of Matlab Toolboxes for fractional order system available, e.g presented in Tepljakov et al. (2011) or Oustaloup et al. (2002).

4. IDENTIFICATION

4.1 Closed Loop Identification of the MLO dynamics

The system of the laser dynamics itself, given in equation (9), is unstable. A PID controller is used to keep the system stable and the response to band limited white noise, added to the reference and the control value, is measured. Using a grey box model with the knowledge of the controller and the structure of the laser plant, leads to the transfer function:

$$G(z) = \frac{-7.384 \cdot 10^{-3}\, z^{-1}}{1 - 1.002\, z^{-1}}\,. \tag{26}$$

4.2 Phase Noise Identification

In order to get the noise transfer functions, the measurements shown in Fig. 6 are used, performed with an Agilent Vector Signal Analyzer (VSA). The parameter of the approximation are determined by minimizing the squared error between the linear approximation and the measurements using the `fmincon` function in Matlab.

The different slopes with the resulting behavior of the MO, dashed line in Fig. 6, are:

Frequency range	Δ dB	α	k
1 kHz − 32 kHz	−26.35 dB	−2.635	−29.38 dB
32 kHz − 501 kHz	−11.84 dB	−1.184	−94.75 dB
501 kHz − 10 MHz	0 dB	0	−162.24 dB

This leads to the filter transfer function

$$W_{r1}(s) = 7.551 \cdot 10^{-9} + \frac{1.943 \cdot 10^{-5}}{s^{0.598} + 1} + \frac{3.495 \cdot 10^{-2}}{s^{1.322} + 1}\,, \quad (27)$$

which has too high amplitudes in the crossing of the linear parts, dash-doted line in Fig. 6. With this starting point an additional optimization leads to the fractional order filter

$$W_{r2}(s) = 7.30 \cdot 10^{-9} + \frac{2.353 \cdot 10^{-4}}{s^{0.847} + 1} + \frac{1.572 \cdot 10^{-1}}{s^{1.540} + 1}\,, \quad (28)$$

which is the solid line in Fig. 6.

The filter for the MLO can be estimated accordingly.

5. SIMULATION RESULTS

To validate the model, the jitter values of the model with the noise shaping filters, calculated by equation (14), are compared to the measured ones of the VSA. In following up papers this is intended to be done using the fractional order frequency limited $\mathcal{H}_2$ norm. The jitter for the MO, in the range of 1 kHz to 10 MHz, is as follows:

$$J_{\text{Measured}} = 16.710\,\text{fs}, \quad J_{\text{Lin.Approx.}} = 16.713\,\text{fs}$$
$$J_{r1} = 18.129\,\text{fs}, \quad J_{r2} = 17.108\,\text{fs}$$

The linear approximation is the best estimation for the jitter, but is not suitable for a common model based controller design. Therefore the filter $W_{r2}(s)$ should be used.

6. CONCLUSION AND OUTLOOK

In this paper a brief overview of the laser based synchronization system for the European XFEL is given. Furthermore, the master laser oscillator is described from the control theory point of view. In order to synthesize an optimal controller it is necessary to model the main factors influencing the system, in this example the phase noise, and the required performance criterion, here the resulting timing jitter. It has been shown, that fractional order systems are appropriate candidates to model the behavior of this noise source. Furthermore, the calculation of the timing jitter can be done by the developed methods.

With a model for that system, the next step is to use modern control synthesis strategies to design a controller which minimizes the output timing jitter. For example due to a minimization of the $\mathcal{H}_2$ norm of performance channels, which include the fractional order noise shape filters.

REFERENCES

Abramovitch, D. (2003). Phase-locked loops: A control centric tutorial. Technical report, Agilent Laboritories, CA, Palo Alto.

Bock, M.K. (2012). *Measuring the Electron Bunch Timing with Femtosecond Resolution at FLASH*. Ph.D. thesis, University of Hamburg.

Brinkmann, R. et al. (2007). The European X-ray free-electron laser technical design report. Technical report, Deutsches Elektronen-Synchrotron.

Chen, Y., Petras, I., and Xue, D. (2009). Fractional order control - a tutorial. In *Proceedings of the American Control Conference*.

Das, S. (2008). *Functional Fractional Calculus for System Identification and Controls*. Springer.

El-Khazali, R., Ahmad, W., and Memon, Z.A. (2007). Noise performance of fractional-order phase-locked loop. In *Proceedings of the International Conference on Signal Processing and Communications*.

Gardner, F. (2005). *Phaselock Techniques*. Wiley.

Günther, C.M., Pfau, B., Mitzner, R., Siemer, B., Roling, S., Zacharias, H., Kutz, O., Rudolph, I., Schondelmaier, D., Treusch, R., and Eisebitt, S. (2011). Sequential femtosecond X-ray imaging. In *Nature Photonics 5*, 99–102.

Kim, J.W. et al. (2004). Large scale timing distribution and RF-synchronization for FEL facilities. *FEL Conference 2004, Trieste, Italy*.

Luo, Y. and Chen, Y. (2012). *Fractional Order Motion Controls*. Wiley.

Monje, C.A., Chen, Y., and Vinagre, B. (2010). *Fractional-order Systems and Controls: Fundamentals and Applications*. Advances in industrial control. Springer.

Oustaloup, A., Melchior, P., Lanusse, P., Cois, O., and Dancla, F. (2002). The CRONE toolbox for Matlab. In *Proceedings of the 41st IEEE Conference on Decision Control*, 240–245.

Oustaloup, A. (1991). Complex non integer derivation in robust control through the CRONE control. In *Analysis of Controlled Dynamical Systems*. Birkhuser Boston.

Pfeiffer, S., Schmidt, C., Lichtenberg, G., and Werner, H. (2011). Grey Box Identification for the Free Electron Laser FLASH exploiting Symmetries of the RF-System. In *Proceedings of the 18th IFAC World Conference*, 10770–10775.

Rubiola, E. (2009). *Phase Noise and Frequency Stability in Oscillators*. Cambridge books online. Cambridge University Press.

Schulz, S. et al. (2013). Past, present and future aspects of laser-based synchronization at FLASH. In *Proceedings of the International Beam Instrumentation Conference 2013*.

Tepljakov, A., Petlenkov, E., and Belikov, J. (2011). FOMCON: Fractional-order modeling and control toolbox for Matlab. In *Proceedings of the 18th International Mixed Design of Integrated Circuits and Systems (MIXDES) Conference*.

Xue, D., Thao, C., and Chen, Y. (2006). Fractional order pid control of a dc-motor with elastic shaft: A case study. In *Proceedings of the 2006 American Control Conference*.